JOURNAL OF MATERIALS SCIENCE 29 (1994) 1958–1965

Metallographic investigation of TiC nucleants in the newly developed Al–Ti–C grain refiner

A. BANERJI, W. REIF
Institut für Metallforschung-Metallkunde, Technische Universität Berlin, W-1000 Berlin 12, Germany

Q. FENG
Department of Materials Science and Engineering, Tsinghua University, Beijing 100084, People's Republic of China

For grain refinement of aluminium and its alloys, a new aluminium-based master alloy containing TiC nucleants was developed a few years ago, by reacting carbon with Al–Ti binary alloy melt. However, as the melt was held at the usual melting temperatures of below 1273 K, the resultant master alloy lost its grain-refining efficiency, and so this phenomenon was called the "poisoning" effect. Nevertheless, a superheating treatment of the melt at higher temperatures (> 1523 K) rejuvenated the nucleant particles. The present investigation, dealing with electron diffraction of carbide particles extracted from the poisoned master alloy, revealed massive formation of Al_4C_3 and Ti_3AlC, of which Al_4C_3 appears to account for the poisoning of TiC nucleants. On the other hand, subsequent electron diffraction studies on the rejuvenated nucleants confirmed that they were essentially composed of uncontaminated TiC.

1. Introduction

TiC has been assumed for a long time to be the nucleant for aluminium inoculated with hypoperitectic titanium concentrations. Following the advent of the "carbide theory" purported by Cibula in 1949 [1], various attempts were made to increase the carbon content of Al–Ti alloy melts in order to generate TiC, which produced little success [2, 3].

Lately, as a result of Banerji's PhD recent work [4], it became possible to produce Al–Ti–C master alloys, both in the laboratory as well as on an industrial scale. These master alloys, which contained 5%–10% Ti and up to about 2% C, showed excellent grain-refining properties comparable to that of Al–Ti–B commercial master alloys and even in some cases the former has been proved to be more effective than the latter [5, 6].

The production of Al–Ti–C master alloys essentially involves reacting carbon particles with an Al–Ti alloy melt under favourable thermochemical conditions to generate *in situ* TiC particulate dispersions in the melt, followed by casting into waffles or producing wires by a subsequent forming operation. These waffles or wires can then be used as an inoculant for aluminium and aluminium alloys, wherein the nucleant is decisively TiC. On the other hand, unfavourable thermochemical conditions prevailing in the melt during the production of master alloys cause poisoning of the TiC particles, which then no longer function as an effective nucleant for the primary aluminium crystals.

The Al–Ti–C master alloys are prepared by reacting graphite or amorphous carbon particles with Al–Ti binary alloy melts, either by using a mechanical stirring process or by induction melting. In general, the alloys contain 5%–10% Ti, up to 2% C, and the rest aluminium. For details of the process of fabrication of these master alloys and their metallographic features, readers are advised to refer to our previous reports [7–9]. However, it may be mentioned here that at the usual melt-processing temperatures, i.e. below 1273 K, the melts are prone to poisoning, so that the resulting cast waffles do not contain active TiC nucleants. Nevertheless, by remelting the poisoned waffles of Al–Ti–C master alloys and providing an optimum superheating treatment to the melt at elevated temperatures sufficiently higher than 1523 K, the active nucleants can be completely restored.

In the present paper, the results of a detailed electron microscopic study of both poisoned and rejuvenated carbide particles have been presented in order to identify the different phases which are formed during the production of the Al–Ti–C master alloys and which directly affect the potency of TiC nucleants.

2. Experimental procedure and results

The microstructure of Al–Ti–C master alloys consists, apart from the acicular $TiAl_3$ primary precipitates, of a particulate phase occurring preferentially at the grain boundary and interdendritic regions. Fig. 1a shows the secondary electron image (SEI) of this finely dispersed phase in the α-Al matrix together with needle-like $TiAl_3$ primary particles. Fig. 1b and c, respectively, show the X-ray mappings of titanium and

0022–2461

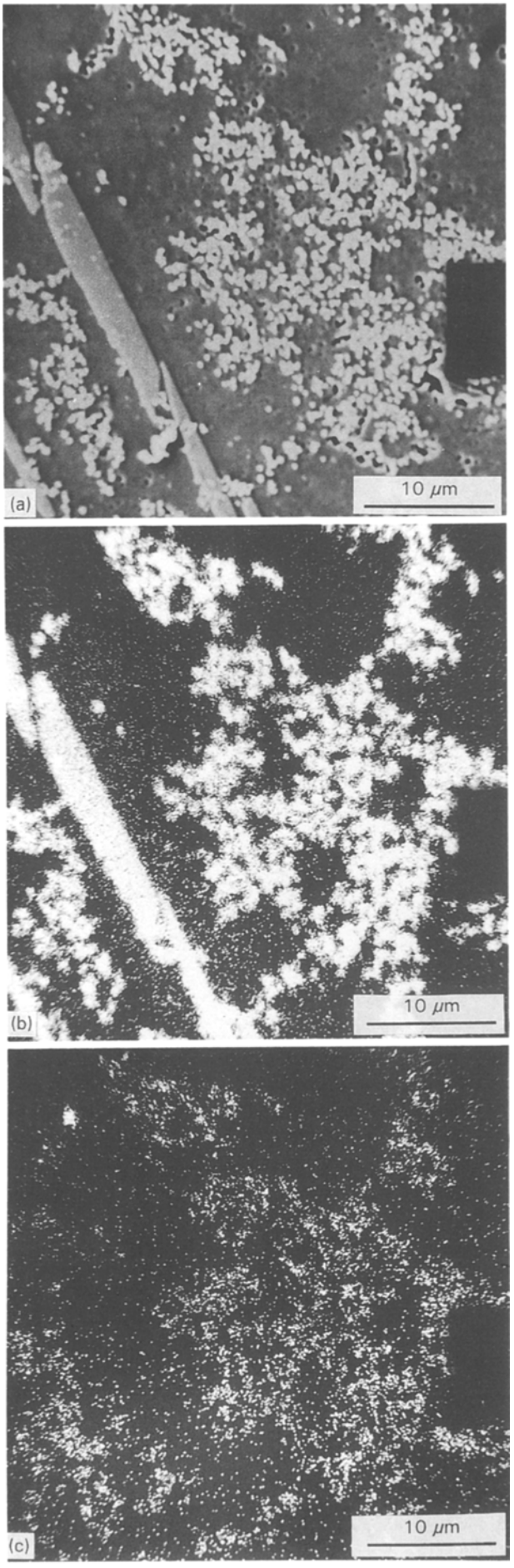

Figure 1 EPMA micrographs of an Al–Ti–C master alloy: (a) SEI picture, (b) Ti X-ray mapping, and (c) C X-ray mapping.

carbon in the region of Fig. 1a. As is evident from the above electron probe microanalysis (EPMA), this particulate phase appears to be essentially composed of titanium and carbon, whereas the needle-like phase is devoid of carbon.

In order to determine their exact structural configuration, these carbide particles were extracted from the matrix and metallographically studied in detail. The two-stage extraction process consisted in initially extracting the carbide particles on a cold-curing resin base, followed by sputtering the replica face with carbon film about 20–30 nm thick. Subsequently, the carbon film was sectioned into 3 mm squares using a sharp knife and the polymer underneath the carbon film was dissolved in a ketone. This left secondary carbon replicas containing the extracted carbide particles. These extraction replicas were then carefully mounted on copper grids for electron microscopic investigation.

The EPMA carried out on the extracted carbide particles provided some useful information which has been summarized in Figs 2–5. Figs 2 and 3 show the typical results of EPMA carried on poisoned TiC particles. Fig. 2a shows the SEI of an extraction replica containing the poisoned carbide particles and Figs 2b and c, the titanium and aluminium X-ray mappings, respectively. It can be seen that these particles also contained, in addition to titanium, a substantially large amount of aluminium. The relative concentrations of titanium and aluminium were, however, non-uniform and varied considerably from particle to particle. This can be apprehended from the non-uniformity of X-ray mapping intensities of titanium (see Fig. 2b) and aluminium (see Fig. 2c) as well as from their much varying relative peak intensities in the energy-dispersive spectral (EDS) analysis carried on different carbide particles and documented in Fig. 3a–c. The peaks of copper (and occasionally also zinc) originated from the grid material used as the specimen holder. Although some particles are richer in titanium and the others in aluminium, nevertheless, both these elements are more or less present in most of the carbide particles. Besides, some small peaks of impurity elements like iron and silicon, of which the former appeared in considerably higher intensities, were frequently observed.

The EPMA results of rejuvenated titanium carbide particles are shown in Figs 4 and 5. Fig. 4a shows a typical SEI picture, and the corresponding X-ray mappings of titanium and aluminium are shown in Fig. 4b and c, respectively. In contrast to the poisoned carbide particles, the rejuvenated titanium carbide particles exhibited essentially the presence of titanium (Fig. 4b) and only some traces of aluminium (Fig. 4c). Compared with the strong peaks of titanium, the peaks of aluminium were only weakly recorded in the EDS analyses, as typically shown in Fig. 5a and b.

Like the poisoned carbide particles, the rejuvenated particles also showed, but in some cases only, the presence of a small amount of the impurity element, silicon. As a contrast, however, no iron peak was recorded. Moreover, unlike the poisoned carbide particles, the EDS analysis of the rejuvenated particles

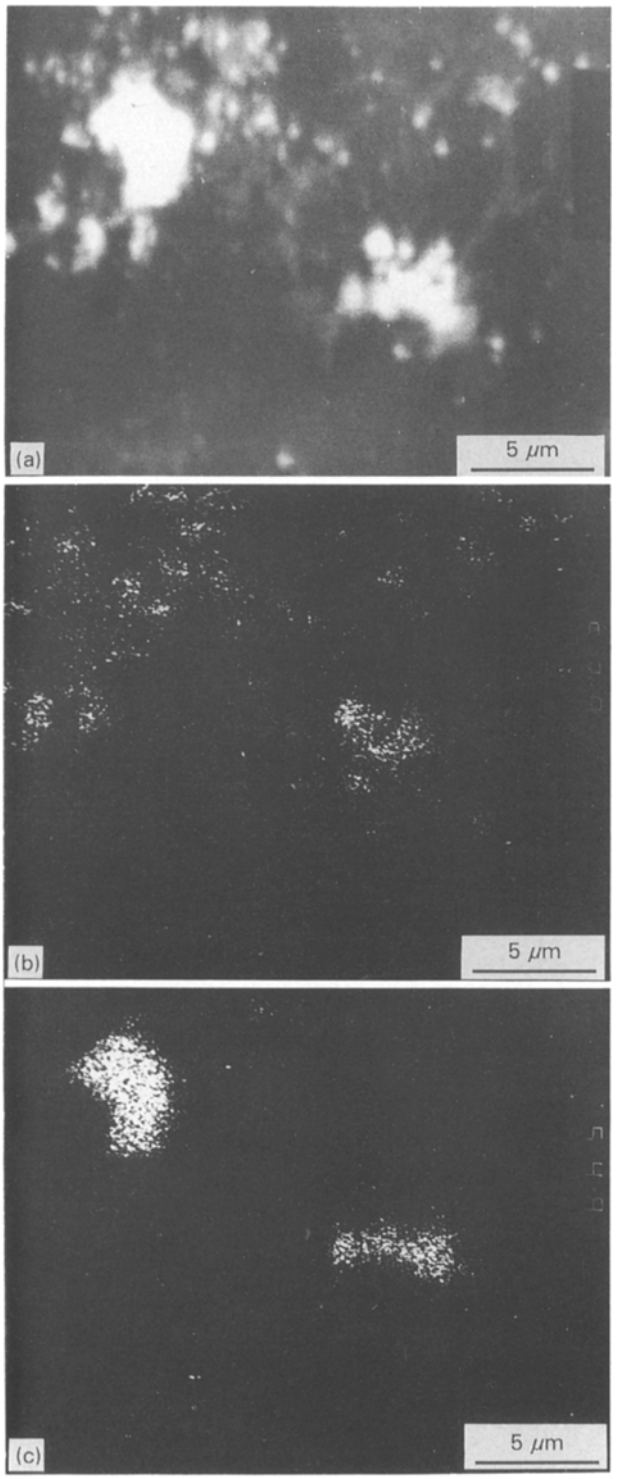

Figure 2 EPMA micrographs of an extraction replica containing poisoned carbide particles: (a) SEI picture, (b) Ti X-ray mapping, and (c) Al X-ray mapping.

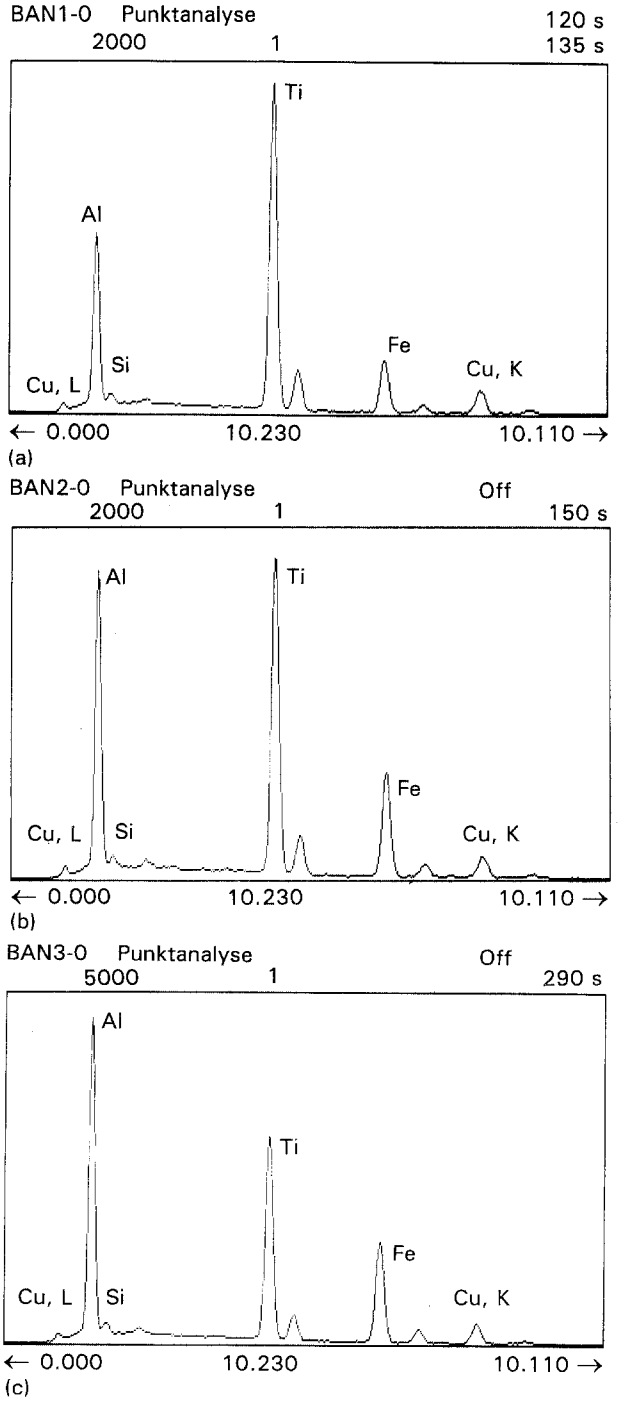

Figure 3 Energy dispersive spectral analyses of different poisoned carbide particles extracted on carbon film.

occasionally showed the presence of some trace elements such as calcium, sulphur and chlorine (see Fig. 5b).

Further investigations of both poisoned and rejuvenated titanium carbide particles were carried out using transmission electron microscopy (TEM). The particles on extraction replicas were extensively diffracted in a 200 kV Jeol microscope. Using lettered grids, it was mostly possible to relocate those particles which were previously analysed with the EPMA. Using the selected-area diffraction technique (SAD), this made it possible to diffract only those particles whose EDS analyses were available. Typical results of the electron diffraction of poisoned and rejuvenated carbide particles are summarized in Figs 6 and 7, as well as in Tables I and II, respectively.

A micrograph showing several poisoned titanium carbide particles is provided in Fig. 6a, and their typical SAD patterns in Fig. 6b and c. On the other hand, Fig. 7a shows the TEM picture of rejuvenated titanium carbide particles, and Fig. 7b and c, the corresponding SAD patterns. The camera constant (λL) was determined by diffracting a standard specimen of polycrystalline thallium chloride. Several specimens of both poisoned and rejuvenated carbide particles were diffracted and more detailed results can

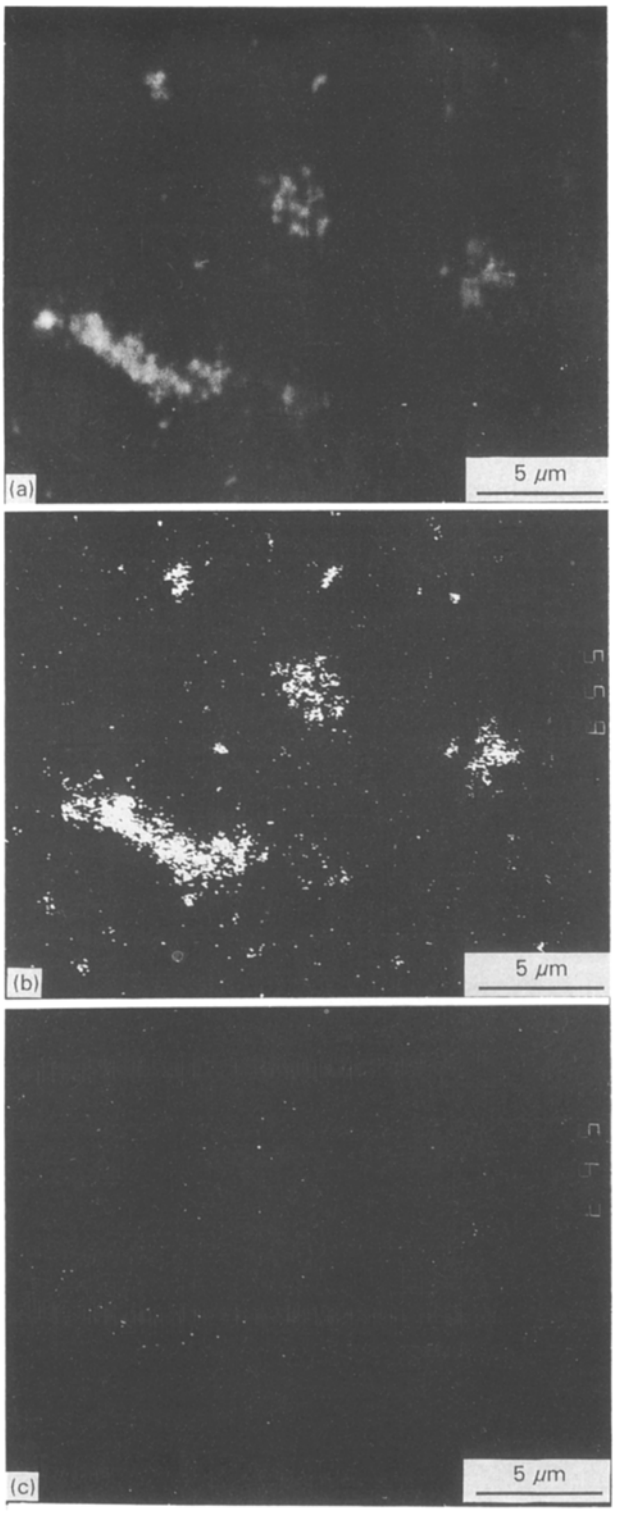

Figure 4 EPMA micrographs of an extraction replica containing rejuvenated carbide particles: (a) SEI picture, (b) Ti X-ray mapping, and (c) Al X-ray mapping.

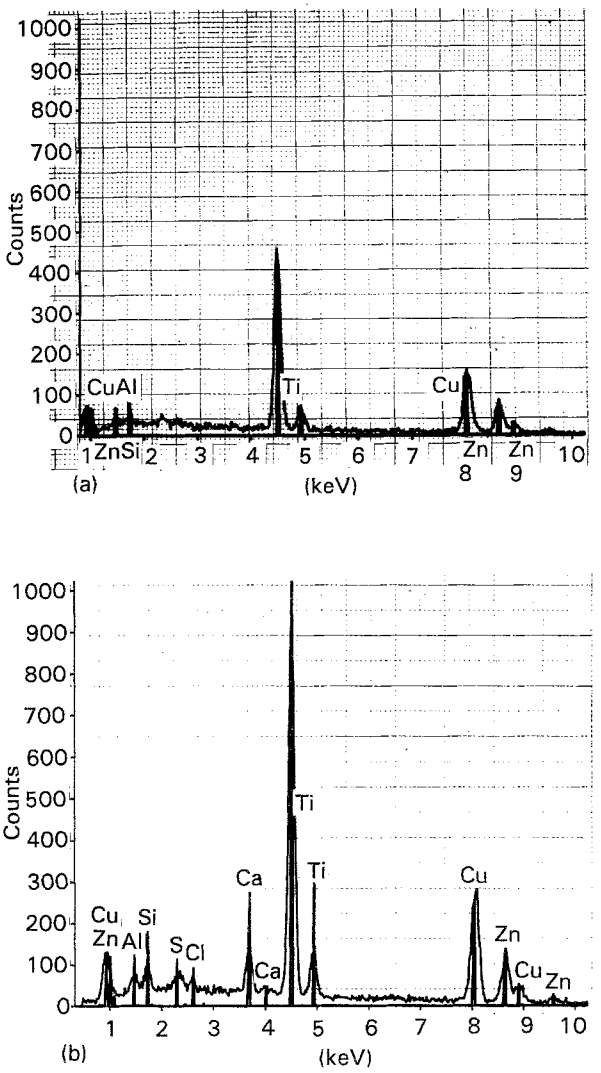

Figure 5 Energy dispersive spectral analyses of rejuvenated carbide particles extracted on carbon film.

be found elsewhere [4]. Here, only typical diffraction data evaluated from the SAD patterns of Figs 6b, c and 7b, c are provided in Tables I and II, respectively.

From Table I, it can be seen that the diffraction patterns of the poisoned carbide particles yielded all the major reflections of TiC, Al_4C_3 and additionally those of the perovskite phase Ti_3AlC [10]. Even very weak reflections of Al_4C_3, such as (1 1 3), (1 2 2) etc., were recorded on the diffraction pattern. As a contrast, the SAD of rejuvenated titanium carbide particles exhibited essentially the reflections of TiC, and only the strongest (1 1 0) reflection of Al_4C_3. The perovskite phase was completely absent in the rejuvenated carbide particles.

Both poisoned and rejuvenated carbide particles yielded reflections at a *d*-spacing of about 0.32 nm, which did not match any reflection of the above three carbide lattices. This, therefore, appears to originate from some impurity phase, which, however, could not be identified and, hence, this reflection as well as another from the poisoned carbides, occurring at a *d*-spacing of about 0.30 nm (possibly of an iron-bearing phase), could not be indexed.

3. Discussion

In our earlier report [8], we suggested, on the basis of metallographic evidence together with consideration of energetical conditions prevailing at the carbon particle/aluminium melt interface, that the reaction of carbon particles with an Al–Ti binary alloy melt at temperatures even below 1273 K caused the formation of TiC particles. In order to confirm that the carbon reacted with titanium of the melt to form TiC first and

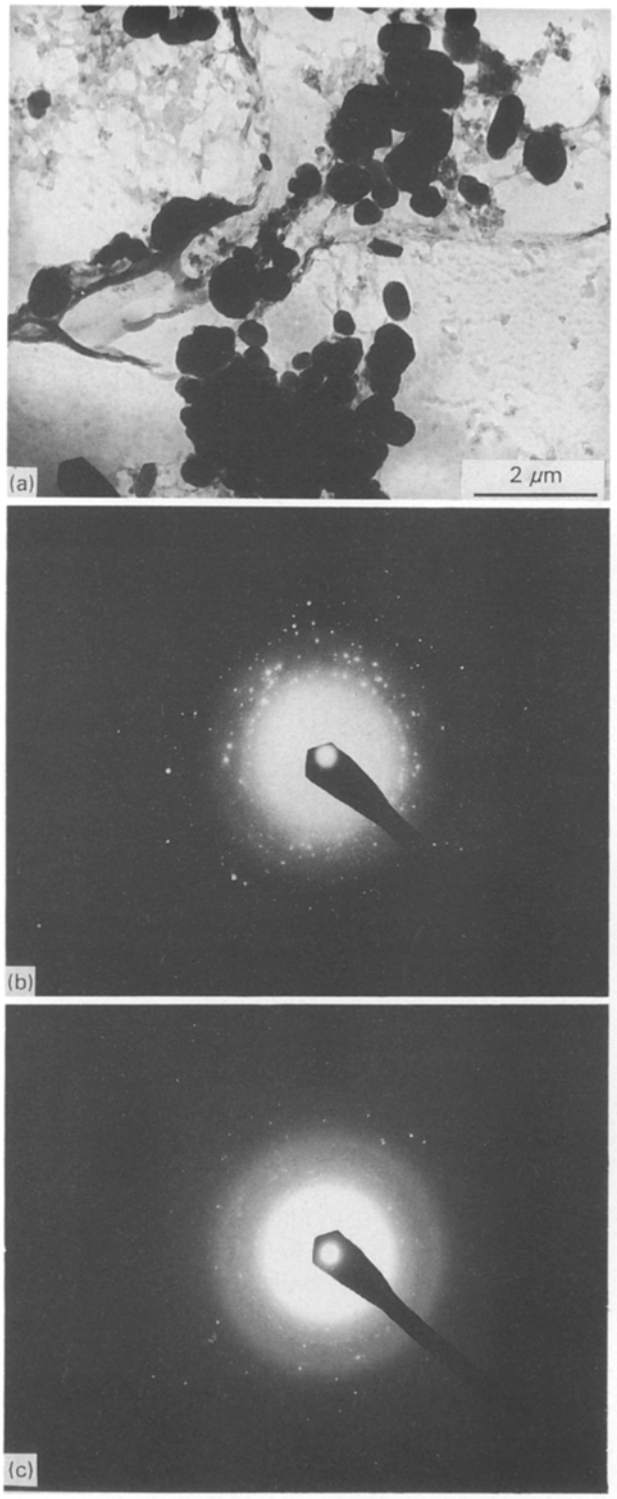

Figure 6 Micrographs of an extraction replica: (a) TEM picture of poisoned carbide particles, and (b, c) typical SAD patterns.

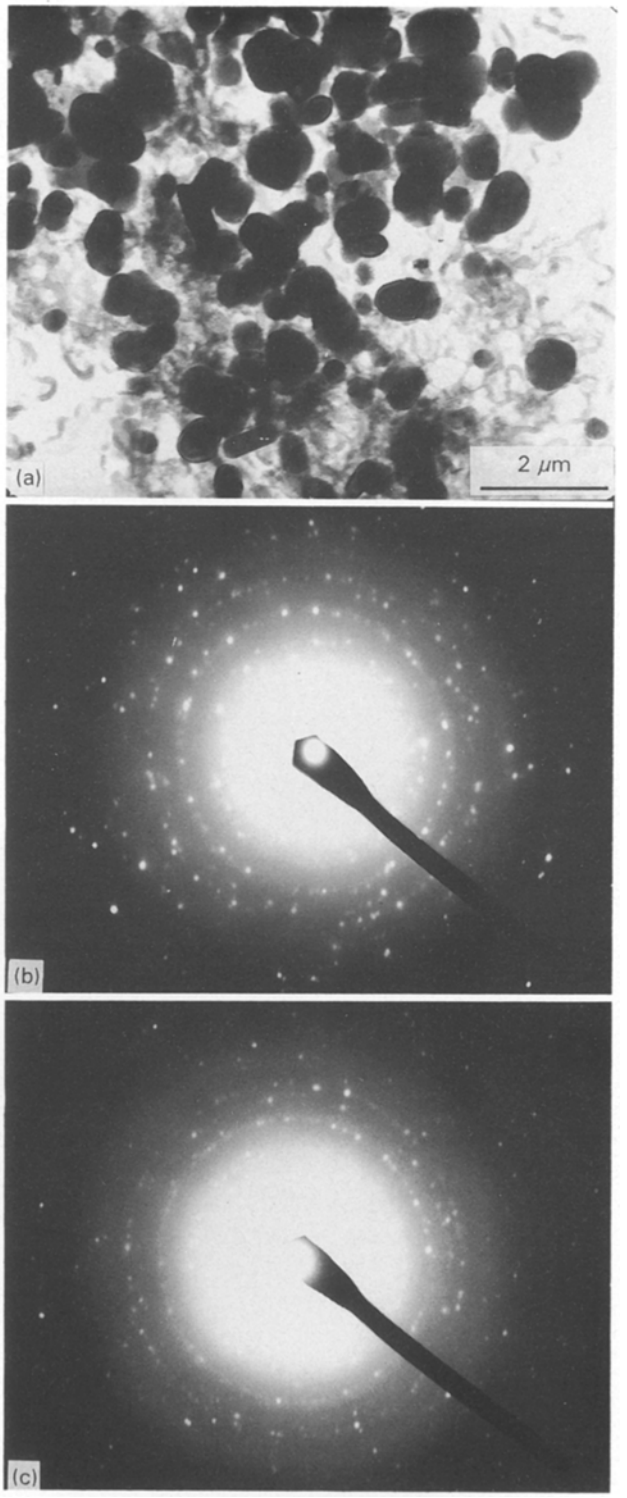

Figure 7 Micrographs of an extraction replica: (a) TEM picture of rejuvenated carbide particles, and (b, c) typical SAD patterns.

not Al_4C_3, melts were quenched before carbon particles could have reacted completely. The resulting microstructures revealed partly reacted carbon particles, which were then analysed using EPMA. Fig. 8 shows a typical result of such microprobe analyses. The SEI micrograph of a partly reacted carbon particle shows a reaction zone at the periphery, constituting the particle/matrix interface (Fig. 8a).

The X-ray mappings of titanium and carbon, provided in Fig. 8b and c, respectively, clearly confirm the onset of reaction of carbon with titanium at the peripheral region and, thereby, the formation of TiC. As the melt was held longer, the reaction was found to proceed further through penetration of the particle by the melt. A typical example of this intermediate reaction stage is provided in Fig. 9a–c. Finally, on holding the melt sufficiently longer, fine particles of TiC were formed and dispersed in the matrix, as typically shown in the micrographs provided earlier in Fig. 1a–c.

These freshly formed TiC particles, however, subsequently reacted with aluminium, thereby forming presumably a sheathing of Al_4C_3 and/or Ti_3AlC, as

TABLE I Evaluation of the diffraction patterns of poisoned carbide particles

Figure	Measured		TiC		Al_4C_3		Ti_3AlC	
	r(mm)	d(nm)	(hkl)	I/I_0	(hkl)	I/I_0	(hkl)	I/I_0
6b	4.45	0.3218	–	–	–	–	–	–
λL = 1.4319 nm mm	4.76	0.3008	–	–	–	–	–	–
	5.71	0.2508	(1 1 1)	80	–	–	–	–
	6.45	0.2220	–	–	(1 0 7)	62	–	–
	6.54	0.2189	(2 0 0)	100	–	–	–	–
	6.98	0.2051	–	–	–	–	200	90
	8.50	0.1685	–	–	(1 1 0)	100	–	–
	8.85	0.1618	–	–	(1 1 3)	2	–	–
	9.60	0.1492	–	–	(0 1 1 4)	12	–	–
	9.80	0.1461	–	–	–	–	220	80
	10.50	0.1364	–	–	(0 0 1 8, 2 0 5)	8	(3 0 0, 2 2 1)	5
	11.00	0.1302	–	–	(0 1 1 7, 2 0 8)	6	–	–
	12.95	0.1106	(4 0 0)	5	(1 2 2)	5	–	–
	13.90	0.1030	–	–	(0 0 2 4)	6	(4 0 0)	20
	14.90	0.0961	(4 2 0)	30	(3 0 0)	6	(3 3 1)	55
	16.05	0.0892	(2 2 4)	30	–	–	–	–
6c	5.74	0.2518	(1 1 1)	80	–	–	–	–
λL = 1.4455 nm mm	6.65	0.2174	(2 0 0)	100	–	–	–	–
	8.55	0.1691	–	–	(1 1 0)	100	–	–
	9.80	0.1475	–	–	–	–	(2 2 0)	80
	10.50	0.1377	–	–	(0 0 1 8, 2 0 5)	8	(3 0 0, 2 2 1)	5
	13.50	0.1071	(4 0 0)	5				

TABLE II Evaluation of the diffraction patterns of rejuvenated carbide particles

Figure	Measured		TiC		Al_4C_3	
	r(mm)	d(nm)	(hkl)	I/I_0	(hkl)	I/I_0
7b	7.80	0.3226	–	–	–	–
λL = 2.5160 nm mm	10.00	0.2516	(1 1 1)	80	–	–
	11.55	0.2178	(2 0 0)	100	–	–
	15.00	0.1677	–	–	(1 1 0)	100
	19.00	0.1324	(1 1 3)	30	–	–
7c	7.85	0.3205	–	–	–	–
λL = 2.5160 nm mm	10.05	0.2503	(1 1 1)	80	–	–
	11.55	0.2178	(2 0 0)	100	–	–
	15.00	0.1677	–	–	(1 1 0)	100
	19.30	0.1304	(1 1 3)	30	–	–

given by the following reversible reactions

$$3TiC + 4Al \rightleftharpoons Al_4C_3 + 3Ti \quad (1)$$

$$9Ti + Al_4C_3 \rightleftharpoons 3Ti_3AlC + Al \quad (2)$$

These carbide particles failed to nucleate aluminium and hence were called "poisoned" carbide particles.

The above predictions (Reactions 1 and 2) have now been fully corroborated by the electron diffraction studies, which confirmed the presence of Al_4C_3 and Ti_3AlC in the poisoned carbide particles (see Table I). Al_4C_3 possesses a hexagonal lattice and its lattice disregistry with aluminium is extremely large. This indicates that the presence of Al_4C_3 would render the carbide particles unsuitable for the nucleation of aluminium. On the other hand, Ti_3AlC possesses a cubic lattice having a minimum lattice disregistry with aluminium of only 2.63%. Therefore, the poisoning of the TiC particles can possibly be attributed to the presence of Al_4C_3 only and not essentially to that of Ti_3AlC.

The rejuvenation process, which consisted in superheating treatment of the melt containing poisoned carbide particles at a temperature sufficiently higher than 1523 K, caused almost complete restoration of the active TiC nucleants. This was clearly evidenced in the results of electron diffraction carried on the rejuvenated TiC particles (see Table II), which showed that these particles were essentially composed of uncontaminated TiC.

Although, some traces of silicon and iron were frequently detected in the EPMA analysis of poisoned carbide particles, their corresponding diffraction patterns, however, failed to provide sufficient evidence of the presence of any known phases containing these elements. One possible reason could be that the concentrations of such phases, if any, in the carbide particles were quite low and, hence, their reflections

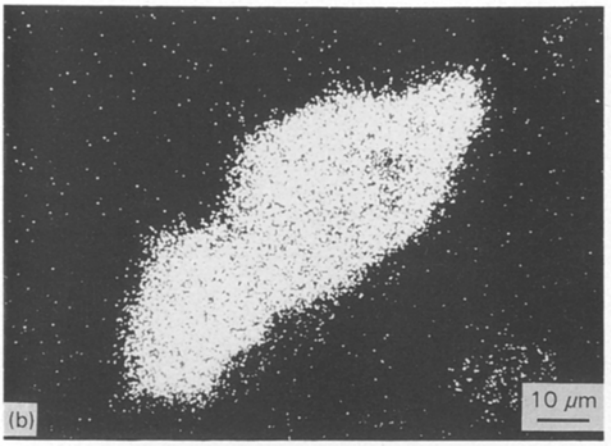

Figure 8 EPMA micrographs showing the onset of reaction of a carbon particle with the titanium of the melt: (a) SEI picture, (b) C X-ray mapping, and (c) Ti X-ray mapping.

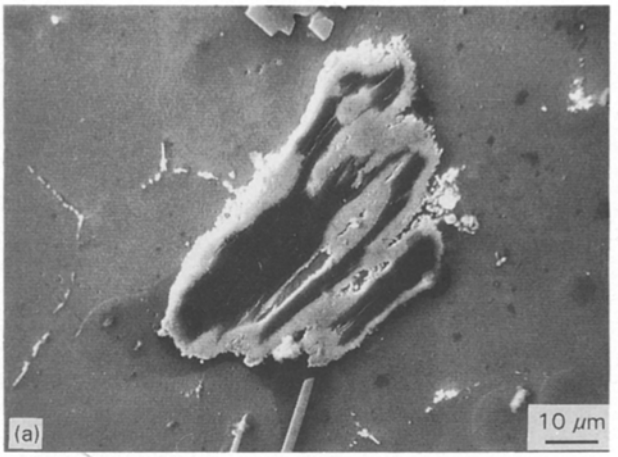

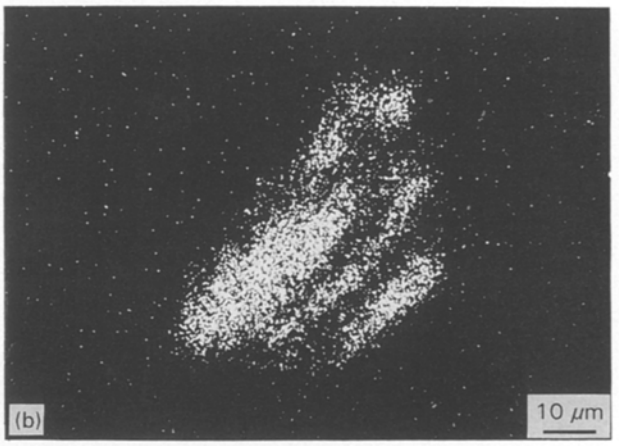

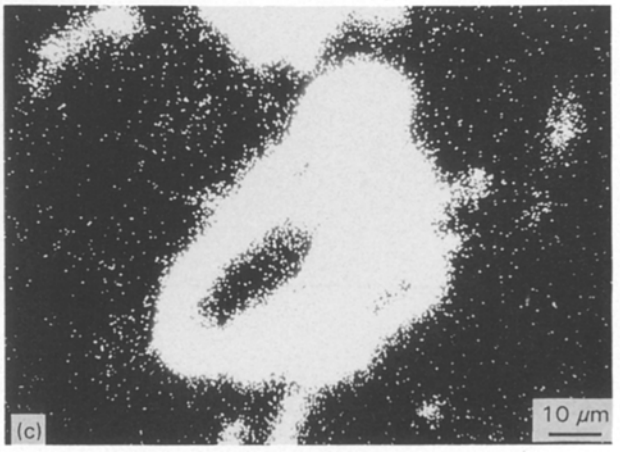

Figure 9 EPMA micrographs showing further reaction through penetration of the carbon particle by the melt: (a) SEI picture, (b) C X-ray mapping, and (c) Ti X-ray mapping.

were too weak to be recorded in the presence of strong reflections from TiC, Al_4C_3 and Ti_3AlC. The other reason could be that these elements possibly dissolved in the carbides without much affecting their lattice geometry.

Both iron and silicon are generally present as impurities in aluminium alloys and, therefore, their presence in the carbide particles is not unlikely. In the present study, however, their roles in the poisoning of carbide particles could not be ascertained. Because silicon was detected only as a trace element, both in the poisoned and rejuvenated particles, it appears that silicon should not be responsible for the poisoning of TiC. On the other hand, as iron was detected in the poisoned carbides only and, in fact, in quite appreciable concentrations, it might also, in addition to Al_4C_3, contribute to the poisoning phenomenon. The roles of other trace elements such as calcium, sulphur and chlorine, which were occasionally detected in the rejuvenated carbides only, are also not clear. Because, they are surface active elements, they are likely to act as surface catalysts during the heterogeneous nucleation process and, hence, their presence cannot be attributed to any poisoning phenomenon.

4. Conclusions

1. During preparation of Al–Ti–C grain refiners, the carbon particles first reacted with titanium of the melt producing TiC particles, which subsequently became poisoned as a result of further chemical reaction with aluminium.

2. The poisoned titanium carbide particles showed the presence of considerable amounts of Al_4C_3 and Ti_3AlC, of which, because of a large lattice misfit with aluminium, Al_4C_3 should be responsible for the poisoning effect.

3. The structural analysis of the rejuvenated carbide particles confirmed that they are essentially constituted of uncontaminated TiC.

4. The reaction sequence (Equations 1 and 2) prevailing in the melt during the production of Al–Ti–C master alloys, which was predicted in an earlier report [8], has been fully corroborated through the results of present metallographic investigation.

Acknowledgement

The authors thank the Centre for Electron Microscopy (ZELMI) for providing assistance with the microscopic work.

References

1. A. CIBULA, *J. Inst. Metals* **76** (1949–50) 321.
2. *Idem, ibid.* **80** (1951–52) 1.
3. J. A. MARCANTONIO and L. F. MONDOLFO, *Metall. Trans.* **2** (1971) 465.
4. A. BANERJI, PhD thesis, Technische Universität Berlin (1987).
5. Q. FENG, PhD thesis, Technische Universität Berlin (1990).
6. A. BANERJI, I.-M. EL HALABI, W. REIF and X.-L. HAN, *Metall.* **44** (1990) 549.
7. A. BANERJI and W. REIF, *Metall. Trans.* **16A** (1985) 2065.
8. *Idem, ibid.* **17A** (1986) 2127.
9. A. BANERJI, W. REIF and London and Scandinavian Metall. Co., Int. Pat. (PCT) WO 86/05212 (1986).
10. W. JEITSCHKO, M. NOWOTNY and F. BENESOVSKY, *Monatsh. Chem.* **95** (1964) 319.

Received 27 August 1992
and accepted 27 September 1993